Surface Manifestations of Internal Waves Investigated by a Subsurface Buoyant Jet: 3. Surface Manifestations of Internal Waves

V. G. Bondur[a], Yu. V. Grebenyuk[a], E. V. Ezhova[b], V. I. Kazakov[b], D. A. Sergeev[b], I. A. Soustova[b], and Yu. I. Troitskaya[b]

[a] *Aerokosmos Scientific Center of Aerospace Monitoring, Gorokhovskii per. 4, Moscow, 105064 Russia*
e-mail: vgbondur@aerocosmos.info

[b] *Institute of Applied Physics, Russian Academy of Sciences, ul. Ul'yanova 46, Nizhny Novgorod, 603950 Russia*
e-mail: yuliya@hydro.appl.sci-nnov.ru

Received August 12, 2009; in final form, February 3, 2010

Abstract—In a large test reservoir at the Institute of Applied Physics, Russian Academy of Sciences, a series of experiments were performed to investigate the surface manifestations of internal waves radiated by a subsurface buoyant jet. The field of currents on the water surface of the reservoir was studied through the distribution of temperature with shallow thermocline. Using Particle Tracking Velocimetry (PTV), the velocity field of surface currents was measured. A theoretical model was developed to calculate the rates of disturbances on the surface. A comparison with experimental data indicated that the calculated data of the surface rate value are overestimated. This discrepancy was explained by the presence of a film of surface-active substances (SASs) with experimentally obtained parameters. Using scale modeling coefficients, we estimated the parameters of internal waves radiated by the subsurface wastewater system and the values of their surface manifestations in field conditions. We estimated the hydrodynamic contrasts in the field of surface waves, which can be caused by these inhomogeneous currents on the surface. For a wind velocity of 5 m/s, the magnitude of the contrast in the field of short waves can reach up to 10−25%, which is detected with confidence by remote-sensing methods.

DOI: 10.1134/S0001433810040079

1. INTRODUCTION

One major trend in the development of advanced methods for studying the coastal water areas is to intensively use remote sensing methods for the sea surface [1, 2]. They are advantageous, first of all, because of the high performance of the monitoring. However, remote sensing methods allow one to obtain only indirect data on oceanic processes. The data interpretation always requires a consideration of the impact that mechanisms of different processes and phenomena in the oceanic thickness make on radar or optical imagery [1].

This study includes a detailed consideration of one of the possible mechanisms of the manifestation of subsurface wastewater sink on the sea surface caused by the radiation of internal waves [1, 3]. The first two parts of this work considered the generation mechanism of internal waves [4] and the structure of the wave field induced by the wastewater system [5]. The main purpose of the third part of this study is to assess the possibility of internal-wave manifestation caused by a subsurface sink on the sea surface. To solve this complex problem, it is necessary to obtain the inhomogeneous current fields created by internal waves on the

sea surface and estimate the hydrodynamic contrasts in the field of surface waves caused by these contrasts.

The currents created by internal waves on the sea surface were investigated on the basis of a scale laboratory simulation at the large thermally stratified tank (LTST) of the Institute of Applied Physics, Russian Academy of Sciences (IAP RAS) [11, 12], as well as using a theoretical model. The experiments involve measurements in the water column and surface. The fields for the water column were described in the second part of this study [5].

The present part of the study considers the measurement results for temperature oscillations in the water column and fields of currents created by these waves on the water surface. The latter was performed using a distribution of temperature with shallow thermocline located at a depth of 13−15 cm on average. The velocities of liquid outflow from the collector model were 40, 70, 100, and 150 cm/s. For these conditions, the Particle Tracking Velocimetry (PTV) method was used to measure the velocities of surface currents.

The theoretical calculations of surface currents were based on the internal-wave model described in the second part of the study [5]. A comparison with

experimental data revealed that this theory overestimates the values of velocities on the surface of fresh water. An explanation for this discrepancy is proposed which is related to films of surface-active substances (SASs) on the water surface. These experiments included measurements of the module of film elasticity and, on that basis, estimates for the surface velocity with regard to its decreased value in the boundary layer, which is caused by the presence of the elastic film. The adjusted estimates of velocity are very consistent with the measurement results.

Based on experimental data coupled with the large laboratory modeling coefficients, we estimated the hydrodynamic contrasts in the field of surface waves with an inhomogeneous current created at the surface by internal waves in field conditions.

This work has the following structure: Section 2 briefly describes the experimental setup for obtaining the velocity field created at the surface by internal waves. Section 3 contains theoretical estimates for the velocity of internal waves at the surface and a comparison with experimental data. Section 4 discusses the role of SAS films at the surface. The theoretical estimates for velocities with account for an SAS film at the surface were compared with the measurement data presented in Section 2. Based on the results of the study, Section 5 estimates the surface manifestations of internal waves in field conditions.

2. A DETERMINATION OF THE FIELD OF VELOCITY CREATED AT THE SEA SURFACE BY INTERNAL WAVES

2.1. Experimental Studies on Measuring the Surface Currents in the LTST for Shallow Thermocline Using the PTV-Method

In the course of experiments on the study of surface currents induced by the collector model in conditions of shallow thermocline (see Fig. 1), the following two important problems have appeared.

The first problem was that, when temperature stratification of the type of a shallow thermocline is created (Fig. 1), large-scale currents as a system of cyclonic and anticyclonic eddies emerge in the surface layer. Measurements performed with the help of the PTV method [6] indicated that the scale of an individual eddy was 1.5−2.5 m, the maximum velocities of currents in it reached 1.3 cm/s, and the average velocities constituted 2−4 mm/s. These values were calculated approximately, because the size of the survey area in both series of experiments did not allow one to cover the whole area occupied by at least one eddy. It can be assumed that eddies appeared by nonuniform horizontal heating of the fine upper layer of stratification. The presence of the eddy current made a low-frequency trend in the dependence of the velocity on time, which was eliminated with the help of the low-frequency filtering of the results (see Subsection 2.2).
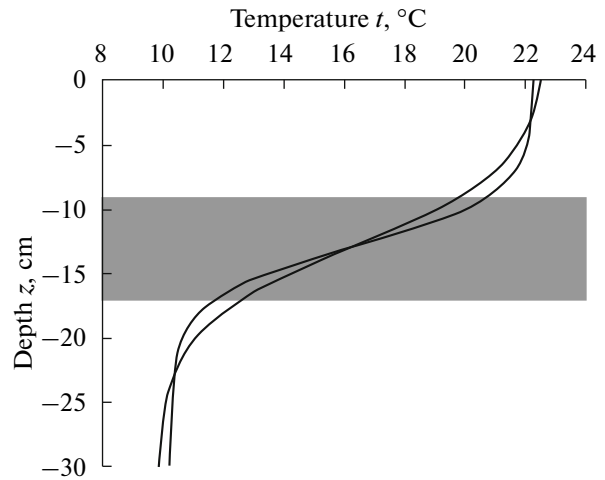

Fig. 1. Operating profiles of temperature stratification in the LTST.

The second factor making it difficult to perform velocity measurements of surface currents is the presence of a SAS film, which could not be completely removed.

We measured the parameters of the SAS film using the technique proposed in [7, 8]. With the help of a special grid, we took samples in the basin and then determined the parameters of the film elasticity by measuring the attenuation of standing capillary−gravitational waves. The relative accuracy of measuring the film-elasticity module by this method constitutes 20%.

A total of four measurements were conducted at the beginning and end of each series of experiments; their results are shown in the table.

The results of measurements of film elasticity modules were used in estimating the velocity at the sea surface (see Section 4).

Table

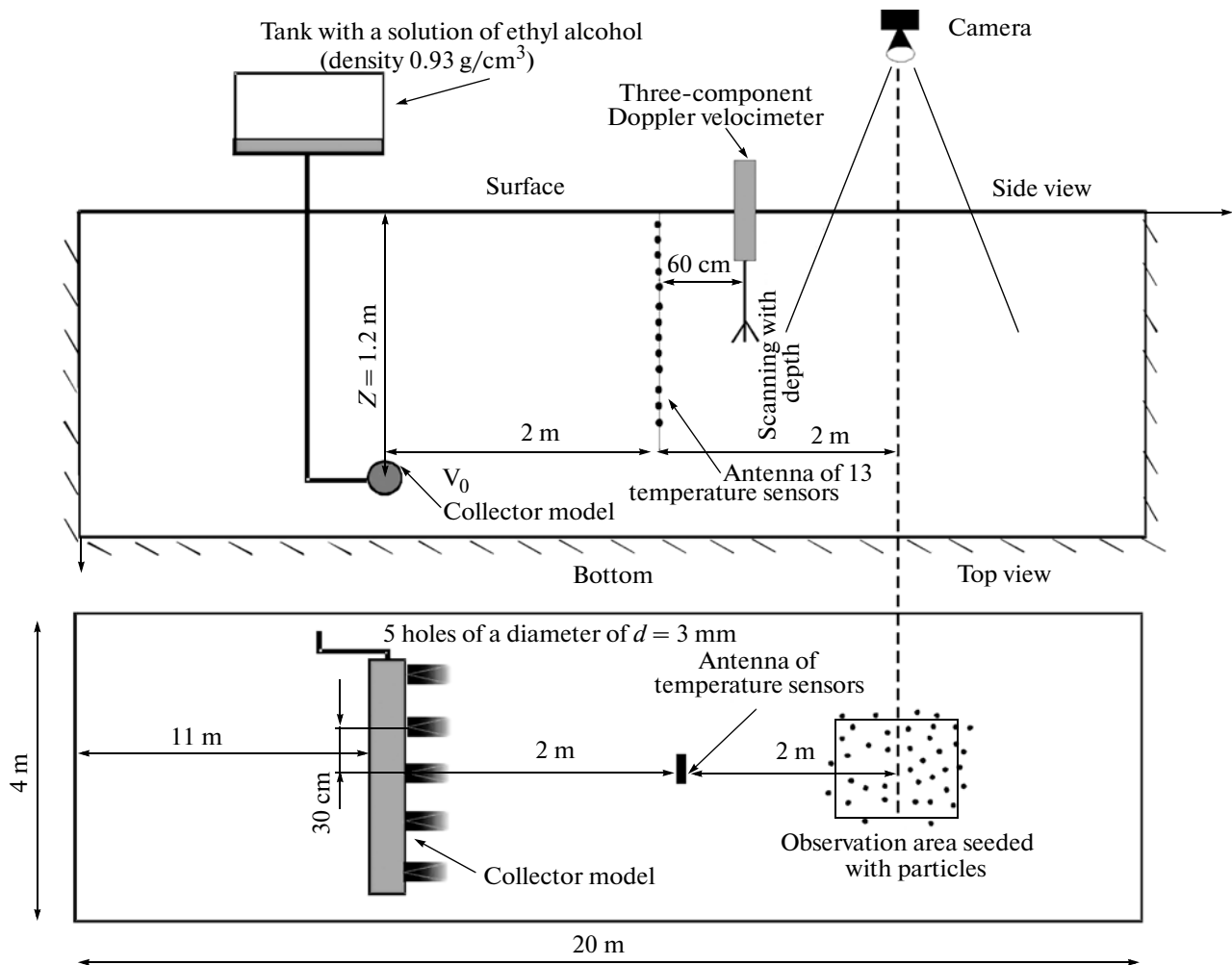| Series of experiments	Surface tension coefficient (dyne/cm)	Elasticity module E (dyne/cm)
Start of series of experiments S1	67.4	2.1
End of series of experiments S1	67	2.8
Start of series of experiments S2	67.5	1.95
End of series of experiments S2	67.1	2.9

Fig. 2. General schematic of LTST IAP RAS experiments with the location of temperature and velocity sensors before the surface observation area (series *S1*).

2.2. Measuring the Velocity at the Water Surface by the PTV Method

As was already mentioned above, in the course of experiments in conditions of stratification with a shallow thermocline [5], the velocity of surface currents induced by buoyant jets was measured with the help of the PTV method [6]. In this case, the limited area of basin surface observation was seeded by particles of black polyethylene with a characteristic size of around 1.5 mm for creating a contrast to the white background of the bottom (see the experimental setups in Figs. 2 and 3). The motion of particles was recorded by a digital video camera from above, and the resulting time series of images were then processed on a computer.

It turned out to be impossible to combine the particle observation area with the sensor allocation area (the distance between sensors and the observation-area center is a minimum) in the conditions of this experiment, because the sensor images hindered the correct identification of particles. In view of this, we

conducted two series of experiments with the sensors and the observation area allocated differently relative to the collector model. The series *S1* (see Fig. 2) included the installation of a vertical antenna of temperature sensors (at a distance of 200 cm from the collector model); a scanning velocity meter (at a distance of 260 cm); and the center of the observation area (at a distance of 400 cm), which is a 60×48 cm rectangle was oriented by its longer side along the direction of the jet current. In the experiment series *S2* (see Fig. 3), the surface observation area was located at a distance of 200 cm from the collector model. The area has dimensions 100×80 cm and was oriented perpendicular to the current motion. Further, at a distance of 300 cm from the collector model, temperature sensors were located and, at a distance of 360 cm, a scanning velocity meter was located.

With the classical PTV-method, one normally measures the velocity of each particle with respect to its motion on frames separated by a time interval and then reconstructs the velocity field by the velocity val-
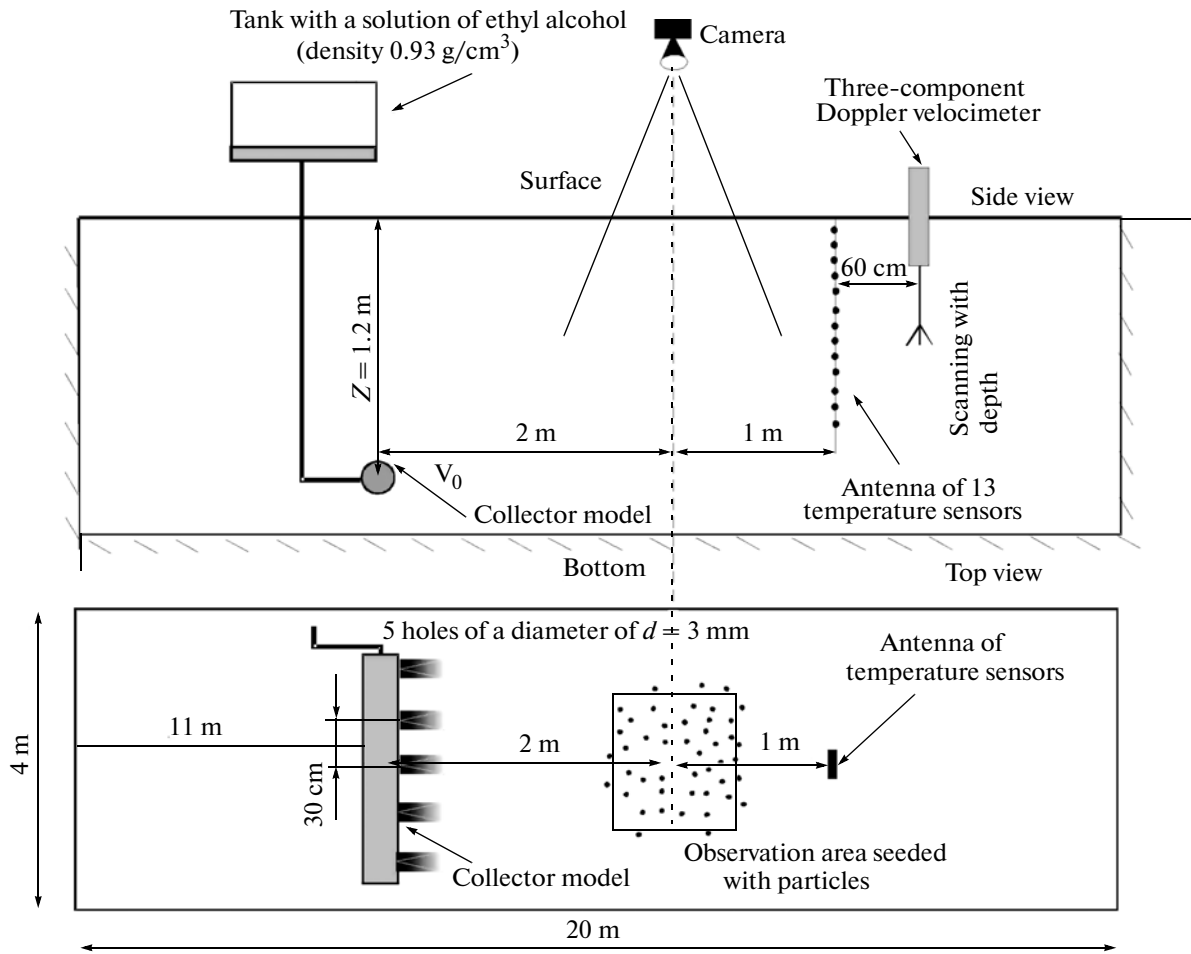
Fig. 3. General schematic of LTST IAP RAS experiments with the location of temperature and velocity sensors beyond the surface observation area (series *S2*).

ues at the points of particle location. In these experiments, due to the presence of a background current (see Subsection 2.1), the number of particles in the observation area quickly decreases with time. For this reason we were able to determine only the averaged (over the observation area) value of the current velocity.

To this end, we found the trajectories of particles passing through this area and calculated their velocity at each moment. Then, at each moment, we calculated the velocity value averaged over all particles that are found in the observation area at the given moment. To exclude the background low-frequency trends in the particle velocity, which are conditioned by the average currents in the basin (see Subsection 2.1), we perform the low-frequency filtering of distributions of signals at frequencies below 0.02 Hz. The examples of such time dependences of averaged (over the observation area) velocities of surface currents are shown in Fig. 4.

Based on measured time realizations, we calculated the rms values of the surface velocity $\langle V'^2 \rangle^{1/2}$. The dependence of $\langle V'^2 \rangle^{1/2}$ on the rate of liquid outflow

from the collector diffuser model is shown in Fig. 5. It can be seen from here that $\langle V'^2 \rangle^{1/2}$ varies in the range between 0.1 and 0.3 mm/s.

3. THEORETICAL ESTIMATES FOR THE RATE OF DISTURBANCES AT THE WATER SURFACE CAUSED BY INTERNAL WAVES WITH UNKNOWN PARAMETERS

Using the representation of the fields of internal waves as expansions with respect to eigenfunctions (see the second part of this study [5]), one can determine the velocity field at the water surface by measured temperature oscillations for known profiles of average temperature and velocity. Indeed, the vertical velocity at any level z can be expressed through a shift of liquid particles according to the formula

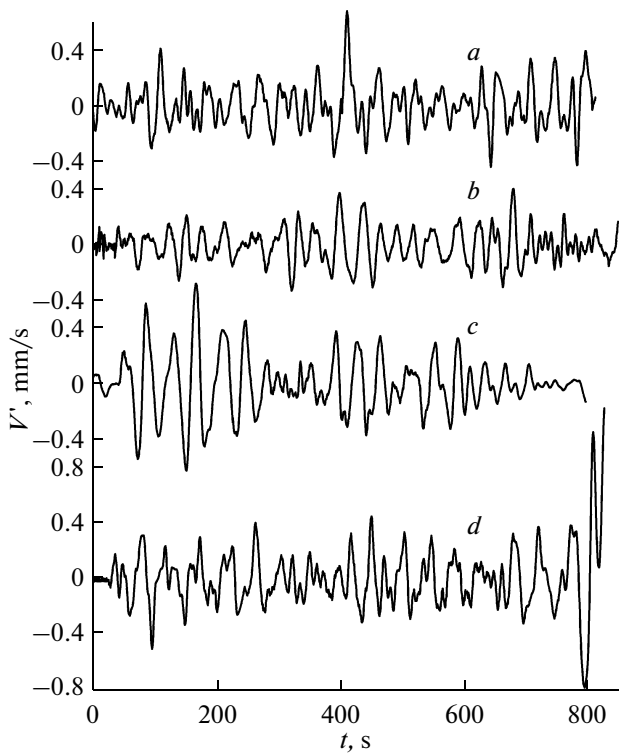$$w = \frac{\partial \xi}{\partial t} + U_0 \frac{\partial \xi}{\partial x} = ik(U_0 - c)\xi. \quad (1)$$

Fig. 4. Rates of disturbances at the basin surface as measured by the PTV method for rates of liquid outflow from the collector model: *a*, 40 cm/s, *b*, 40 cm/s, *c*, 100 cm/s, and *d*, 150 cm/s.

Fig. 5. Standard deviations of velocities of surface currents (the squares indicate the *S1* series and the diamonds indicate the *S2* series).

Then, in view of relations

$$w = -\frac{\partial \psi}{\partial x} = -ik\psi = ik(U_0 - c)\xi,$$

$$\psi = -(U_0 - c)\xi, \tag{2}$$

$$u = \frac{\partial \psi}{\partial z},$$

one easily can derive the expression for the horizontal velocity u of particles through the shift ξ:

$$u(z, t) = (c - U_0)\frac{\partial \xi}{\partial z} - \xi\frac{dU_0}{dz}. \tag{3}$$

In the second part of this study [5], it was shown that the field of internal waves can be represented as a superposition of the first two modes of internal waves. Then, one can represent the relation for the shift of liquid particles as the expansion

$$\xi(z, t) = A(t)\varphi_1(z) + B(t)\varphi_2(z), \tag{4}$$

where $\varphi_1(z)$, $\varphi_2(z)$ are the first and second eigenmodes of the system. Because the derivative of the average
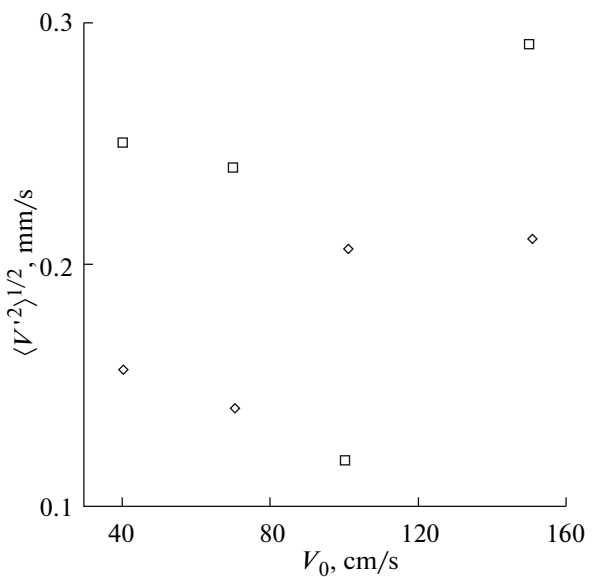
velocity at the water surface is equal to zero, $\frac{dU_0}{dz}\big|_{z=0} = 0$, we obtain

$$u\big|_{z=0} = u_0 = A(t)(c_1 - U_0)\frac{d\varphi_1}{dz}\big|_{z=0}$$

$$+ B(t)(c_2 - U_0)\frac{d\varphi_2}{dz}\big|_{z=0}, \tag{5}$$

where c_1 and c_2 are the phase velocities of the first and second eigenmodes, respectively.

As was noted in Section 2, the signal processing at the basin surface is performed through low-frequency filtering with a frequency cutoff of 0.02 Hz. This technique was applied to each isotherm in all experiment realizations; next, the field of isotherm shifts was expanded with respect to modes and the time dependences $A(t)$ and $B(t)$ of expansion coefficients by modes were determined. The values of derivatives of eigenfunctions at the surface were found by solving the boundary problem for eigenfunctions and eigenvalues (see formulas (6) and (7) in [5]). Using the resulting relations and on the basis of formula (5), we calculated the time dependences of the velocity of the surface currents. Then they were compared with the results of measurements of the surface currents with the help of the PTV-method.

Figures 6 and 7 show the dependences of the average velocity amplitude of surface currents on the rate of liquid outflow from the collector model, which were obtained theoretically and experimentally. It can be seen from these figures that the theoretical estimates considerably exceed the experimental results (by about 2–5 times). This discrepancy can be explained
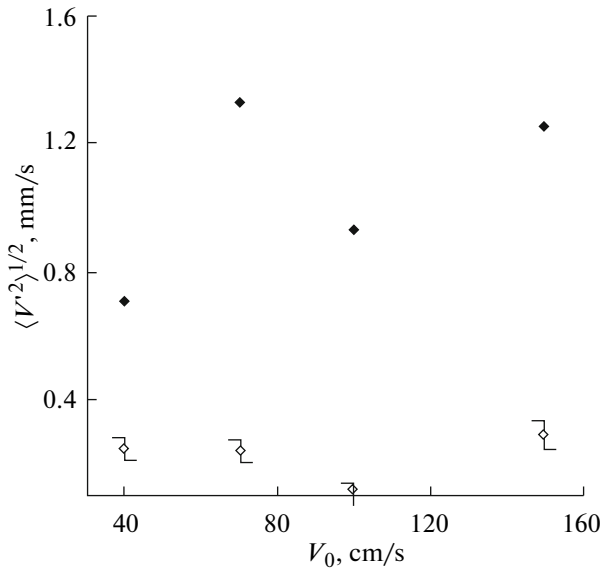
Fig. 6. Standard deviations of the velocities of surface currents (series *S1*): the black diamonds indicate theoretical estimates without accounting for the influence of the film and the light diamonds indicate the measurement results obtained by the PTV method.

Fig. 7. Standard deviations of the velocities of surface currents (series *S2*): the black diamonds indicate theoretical estimates without accounting for the influence of the film and the light diamonds indicate the measurement results obtained by the PTV method.
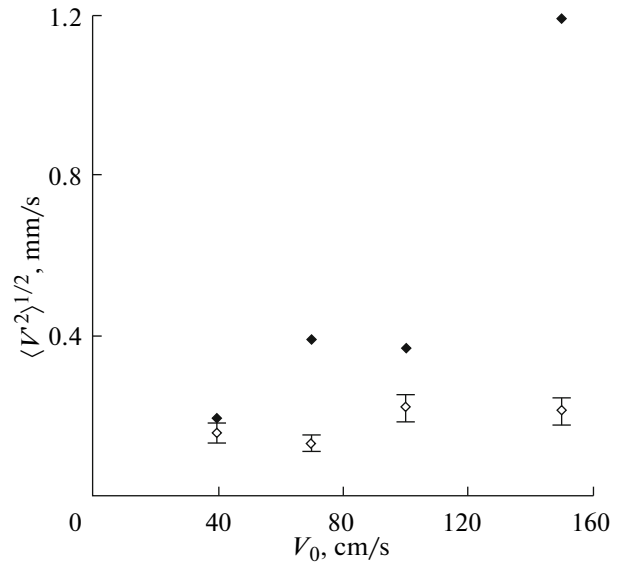
by the presence of the SAS film at the water surface (the film-elasticity modules measured experimentally are presented in the table).

4. ESTIMATION OF THE INFLUENCE OF SAS FILMS ON WATER SURFACE

When a SAS film is present near the water surface, a wave boundary layer is generated with a significantly changed liquid velocity when compared to its value outside the boundary layer. To describe the change in the structure of the internal-wave mode when a SAS film is present, one needs to take into account the molecular viscosity of water. In this case, the free surface of water requires an additional boundary condition for the continuity of tangential stresses with account for the film elasticity [9]:

$$\nu\left(\frac{\partial w}{\partial x} + \frac{\partial u}{\partial z}\right) = -\frac{d\sigma}{d\Gamma}\frac{\partial \Gamma}{\partial x}, \tag{6}$$

where σ is the coefficient of surface tension, Γ is the surface concentration of the SAS film, and ν is the coefficient of molecular viscosity.

The scale of wave boundary layer δ is determined by the wave frequency ω and molecular viscosity ν:

$$\delta = \sqrt{\frac{\nu}{\omega}}, \tag{7}$$

here, for internal waves in the LTST, the following condition is satisfied:

$$k\delta \ll 1. \tag{8}$$

In this case, the problem of the influence of the SAS film on the structure of internal waves can be solved by the method of joined asymptotic expansions [10]. In this case, the wave field outside the boundary layer is described by the system of equations of ideal hydrodynamics of a stratified liquid (external solution) [11] and, inside the boundary layer, the disturbances of horizontal velocity u satisfy the diffusion equation (internal solution):

$$\frac{\partial u}{\partial t} = \nu\frac{\partial^2 u}{\partial z^2}. \tag{9}$$

The joining of the external and internal solutions yields the boundary condition for equation (9) as $z \longrightarrow \infty$:

$$u\big|_{z \to \infty} = U_0 e^{-i(\omega t - kx)}, \tag{10}$$

where U_0 is given by formula (5).

If condition (8) is satisfied, boundary condition (6) takes the form

$$\nu\left(\frac{\partial u}{\partial z}\right) = -\frac{d\sigma}{d\Gamma}\frac{\partial \Gamma}{\partial x}.$$

Applying the equation for the surface concentration of SAS [9],

$$\frac{\partial \Gamma}{\partial t} + \frac{\partial}{\partial x}(\Gamma_0 u) = 0,$$

we finally obtain the boundary condition to perturbations of the horizontal velocity at the surface:

$$\nu\left(\frac{\partial^2 u}{\partial t \partial z}\right) = E\frac{\partial^2 u}{\partial x^2}\bigg|_{z=0}, \tag{11}$$

where $E = -\Gamma_0 \dfrac{d\sigma}{d\Gamma}$ is the module of film elasticity.

The solution of Eq. (9) with boundary condition (10) has the form

$$u(x, z, t) = \left(U_0 + U_\nu \exp\left(\frac{1+i}{\sqrt{2}}\sqrt{\frac{\omega}{\nu}}z\right)\right)e^{-i(\omega t - kx)}. \quad (12)$$

Inserting the solution of (12) into boundary condition (11), we obtain

$$U_\nu = \frac{U_0\left(1 - \sqrt{\left(\dfrac{Ek^2}{\sqrt{\omega^3\nu}} + \dfrac{1}{\sqrt{2}}\right)^2 + \dfrac{1}{2}}\right)}{\sqrt{\left(\dfrac{Ek^2}{\sqrt{\omega^3\nu}} + \dfrac{1}{\sqrt{2}}\right)^2 + \dfrac{1}{2}}}. \quad (13)$$

Then, the amplitude $U_0 + U_\nu$ of horizontal velocity induced by an internal wave at the water surface in the presence of a SAS film will be expressed as

$$U_0 + U_\nu = \frac{U_0}{\sqrt{\left(\dfrac{Ek^2}{\sqrt{\omega^3\nu}} + \dfrac{1}{\sqrt{2}}\right)^2 + \dfrac{1}{2}}}. \quad (14)$$

Theoretical estimations of the value of the velocity on the surface according to formula (14) were compared to the measurement data (Figs. 8, 9). The values of modules of elasticity E used for the estimation are shown in the table. The estimate for the error in theoretical values was determined by the measurement error of E, which constituted 20% [7, 8]. It is seen from the figures that the resulting theoretical estimates are in significantly better agreement with experimental data than in Figs. 6 and 7.

Thus, the experiments revealed that, in the presence of internal waves radiated during the liquid outflow from the subsurface collector model, surface currents with spatial periods controlled by the lengths of internal waves appear. Their scales are indicated in Table 2 of the second part of this work [5] and constituted 30 to 60 cm. The standard deviations of velocities in the presence of a SAS film at the water surface take values in the range from 0.1 to 0.3 mm/s, which correspond to the amplitudes from 0.15 to 0.45 mm/s. A comparison with Fig. 5 indicates that these values for a pure water surface would constitute 1 to 2 mm/s.

It should be pointed out that these experiments were performed for conditions of scaled modeling. In view of this, using the coefficients of modeling [12], one can estimate the currents created near the subsurface collector in field conditions, the parameters of radiated internal waves, and the value of their surface manifestations, as well as make conclusions on the possibility of remote diagnostics of these waves. In our laboratory experiment, the coefficient of scale modeling with respect to the velocity value constitutes 1 : 3 and the coefficient of geometric similarity was 1 : 27. In view of this, we reveal the fact that this experiment

simulated stratification with a pycnocline thickness of around 4 m, an internal-wave length of 8 to 43 m, a wave phase velocity of 5 to 10 cm/s, and a surface velocity of 0.3 to 0.6 cm/s.

5. ON THE POSSIBILITY OF REMOTE DIAGNOSTICS OF SURFACE MANIFESTATIONS OF INTERNAL WAVES

Let us estimate the hydrodynamic contrasts in the field of surface waves, which can induce surface currents with the velocities determined in Section 4. To this end, we use the kinetic equation for the spectral density of wave action

$$N(k) = E(k)/\Omega_0(k), \quad (15)$$

where $\Omega_0(k)$ is the proper frequency of waves and $E(k)$ is the wave-energy spectrum [13]:

$$\frac{\partial N}{\partial t} + \frac{\partial \Omega}{\partial k}\frac{\partial N}{\partial x} - \frac{\partial \Omega}{\partial x}\frac{\partial N}{\partial k} = B[N, U]N + \text{Int}[N], \quad (16)$$

where $B[N, U]$ is the wave increment depending on the heaving spectrum, N and U are parameters characterizing the wind velocity (hereafter, U is represented as u_*^2: the square of viscous friction velocity, which is proportional to tangential turbulent stress), Ω is the circular frequency, k is the wave number, and $\text{Int}[N]$ is the collision integral determining the nonlinear interaction of waves.

If there is a surface current field u_{1w}, generated by internal waves, it produces disturbances in the surface-wave distribution N_1. If they are small in comparison with undisturbed values $N = N_0$, one can use these values to expand $B[N, U]$ and $\text{Int}[N]$ into a Taylor series.

Taking into account the Doppler effect, the circular frequency of surface waves with a wave number k in the laboratory system of reference can be expressed as

$$\Omega = \Omega_0(k) + ku_{1w}(x, t), \quad (17)$$

where $\Omega_0(k)$ is a dispersion equation for gravitational–capillary waves on the resting mode.

The expressions for the collision integral in the right-hand side of (16) are well known (see, for example, [13]) but complicated for using in applications. A number of authors used different modifications of the so-called relaxation models for approximating the collision integral in (16) [14, 15]. Let us use the model proposed in [16].

Let $N_0(k)$ be a equilibrium spectrum of wind waves. It satisfies the equation

$$B[N_0, U] + \text{Int}[N_0] = 0. \quad (18)$$

Let us consider a spatially homogeneous disturbance N_1 of the equilibrium spectrum $N_0(k)$ of wind
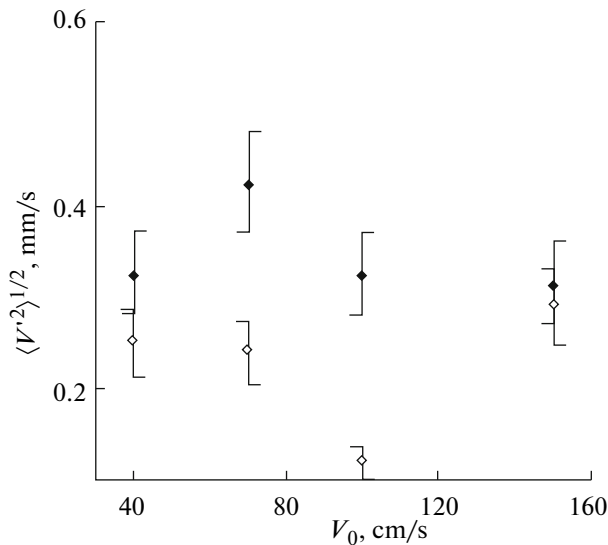
Fig. 8. Standard deviations of velocities of surface currents (series *S1*): the black diamonds indicate theoretical estimates while accounting for the influence of the film and the light diamonds indicate the measurement results obtained by the PTV method.
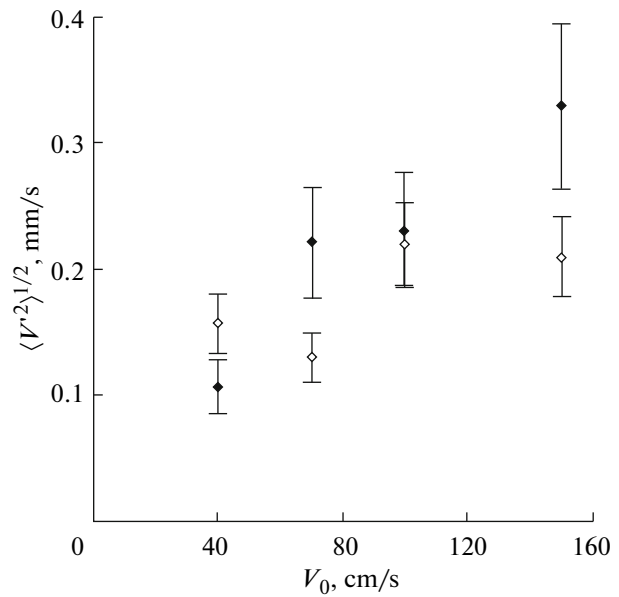

Fig. 9. Standard deviations of the velocities of surface currents (series *S2*): the black diamonds indicate theoretical estimates while accounting for the influence of the film and the light diamonds indicate the measurement results obtained by the PTV method.

waves. Then, $N = N_0 + N_1$. If $N_1 \ll N_0$, equation (16) can be linearized:

$$\frac{\partial N_1}{\partial t} = \frac{\delta}{\delta N_0} B[N_0] N_1 N_0$$
$$+ B[N_0] N_1 + \frac{\delta}{\delta N_0} \text{Int}[N_0] N_1. \tag{19}$$

The solution of (19) can be sought in the form

$$N_1 = N_{10}(k) \exp(-\beta_r(k)t), \tag{20}$$

where $\beta_r(k)$ is the relaxation rate. Inserting (20) into (19), we obtain

$$-\beta_r N_1 = \left[\frac{\delta}{\delta N_0} B[N_0] N_0 \right.$$
$$\left. + B[N_0] + \frac{\delta}{\delta N_0} \text{Int}[N_0] \right] N_1. \tag{21}$$

The expression in square brackets is an operator and β_r is its eigenvalue. For the disturbance of the collision integral, a relaxation approximation was proposed [15]:

$$\frac{\delta}{\delta N_0} \text{Int}[N_0] N_1$$
$$= \left[-\frac{\delta}{\delta N_0} B[N_0] N_0 - B[N_0] - \beta_r \right] N_1. \tag{22}$$

Using approximation (22) and expression (17) for Ω, we obtain from (19)

$$\frac{\partial N_1}{\partial t} + \upsilon_{gr} \frac{\partial N_1}{\partial x} - k \frac{\partial u_{w1}}{\partial x} \frac{dN_0}{dk} = -\beta_r N_1. \tag{23}$$

For simplicity, we assume that the dependence of u_{1w} on x is harmonic:

$$u_{1w} = u_{10w} e^{-i(\omega t - qx)}; \tag{24}$$

then,

$$N_1 = N_{10} e^{-i(\omega t - qx)}. \tag{25}$$

Inserting (24) and (25) into (23), we obtain

$$N_{10} = \frac{iq u_{10w} k \dfrac{dN_0}{dk}}{iq \left(\dfrac{d\Omega_0}{dk} - \dfrac{\omega}{q} \right) + \beta_r}. \tag{26}$$

As the relaxation time, the authors of [15] recommend taking a value proportional to the rate that the density of the surface-wave energy rises with a coefficient of $2-5$. We used the Plant formula [16] and took a proportionality coefficient of 2. Then, we have

$$\beta_r = 0.08 \frac{u_*^2}{c^2} \Omega_0, \tag{27}$$

where $c = \sqrt{g/k + \sigma k}$; $\Omega_0 = \sqrt{gk + \sigma k^3}$. Let us assume that the form of the surface-rise spectrum in surface waves is described by the Phillips saturation spectrum [17] $E(k) = \alpha k^{-4}$, then, the spectrum of wave action is

$N_0(k) = E(k)/\Omega_0(k) = \alpha k^{-4}/\sqrt{gk + \sigma k^3}$. In view of this, one can use (26) to estimate the coefficient of modulation of spectral density of the harmonics with wave number k:

$$M(k) = \frac{N_{10}}{N_0}$$

$$= -\frac{iu_{10w}\left(4 + 0.5\left(g + 3\sigma k^2\right)/\left(g + \sigma k^2\right)\right)}{i\left(\dfrac{g + 3\sigma k^2}{2\sqrt{gk + \sigma k^3}} - \dfrac{\omega}{q}\right) + 0.08\dfrac{u_*^2 k^2}{q\sqrt{gk + \sigma k^3}}}. \qquad (28)$$

The dependence graph of the module of modulation coefficient $|M(k)|$ is shown in Fig. 10 for the following parameters of internal waves and surface currents: $\omega/q = 9.6$ cm/s, $u_* = 18$ cm/s (the wind velocity is around 5 m/s), $u_{10w} = 0.6$ cm/s (solid line) and $u_{10w} = 0.3$ cm/s (dotted line). It can be seen that the contrast maximum $(0.035{-}0.07)$ is reached at $k = 0.12$ cm^{-1} (a wavelength of around 50 cm). These contrasts can be marked out by using the spatial spectral processing of images [1, 2].

One may expect a rise in the hydrodynamic contrast at short nonlinear waves that are the harmonics of decimeter-range waves (the so-called bound waves) [18, 19]. For these waves, on the basis of laboratory experiments [20, 21], a sharp increase in the contrast of centimeter and millimeter ranges was revealed over decimeter waves in the presence of inhomogeneous currents. These studies noticed a 7–8-fold increase in coefficients of modulation of centimeter and millimeter waves when compared to decimeter waves. If these values are used for estimating, one can expect high hydrodynamic contrasts in the connected centimeter and millimeter waves on an order of 0.25–0.6. It should be noted that, in field conditions, the field of wind waves includes (together with connected short waves) free waves which are weakly modulated in the presence of the internal waves considered here for two reasons: the strong renewal from the group resonance and the small relaxation time. According to Plant's measurements [22], the fraction of bound waves for a wind velocity of 5 m/s is equal to 0.5. This yields an estimate for the contrast in the field of short waves of 0.12–0.3, which can be confidently detected with the help of remote methods [1, 2].

CONCLUSIONS

To investigate the surface manifestations of deep-water sinks in the large thermally stratified basin at the Institute of Applied Physics, Russian Academy of Sciences, a scale simulation was performed to actuate internal waves by turbulent buoyant jets flowing from the diffusers of subsurface wastewater systems in conditions of temperature stratification with shallow thermocline.
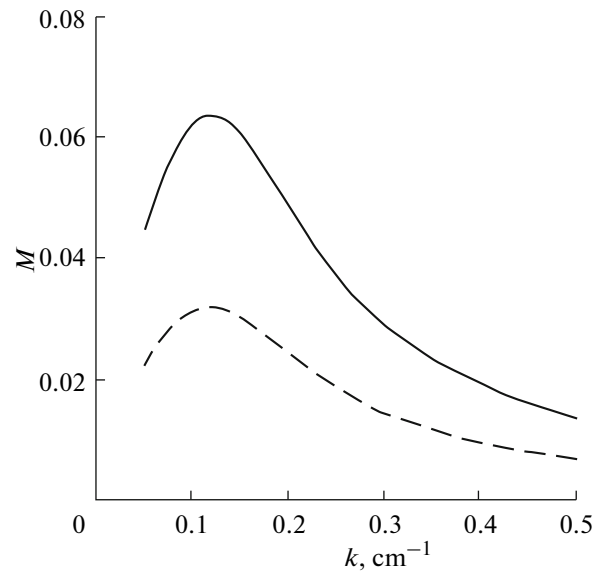
Fig. 10. Graph of the dependence of the modulation coefficient of short waves $M(k)$ for the following parameters of internal waves at the surface: $\omega/q = 9.6$ cm/s, $u_* = 18$ cm/s, $u_{10w} = 0.6$ cm/s (solid line), and $u_{10w} = 0.3$ cm/s (dashed line).

Using the PTV method, the velocities of currents generated by internal waves at the water surface in the basin were measured. The values of surface velocities in this laboratory experiment were significantly reduced due to the presence of a SAS film, which could not be eliminated completely. In relation to this, special measurements of the film parameters were performed and its influence on the surface velocities was estimated. For the known parameters of the film, it became possible to estimate the velocities that would be generated by internal waves at the surface of pure water. The amplitudes of velocity oscillations estimated in this way were equal to 0.1–0.2 cm/s.

Using the coefficients of scale modeling, we estimated the parameters of internal waves (particularly with wavelengths varying in the range between 8 and 45 m) radiated by a subsurface wastewater sink and the values of their surface manifestations in field conditions. We estimated the hydrodynamic contrasts in the field of surface waves, which can be caused by these inhomogeneous currents on the surface. For a wind velocity of 5 m/s, the magnitude of the contrast in the field of short waves can reach up to 10–25%, which is detected with confidence by remote-sensing methods.

ACKNOWLEDGMENTS

REFERENCES

1. V. G. Bondur, "Aerospace Methods in Modern Oceanology," in *New Ideas in Oceanology*, Vol. 1: *Physics. Chemistry. Biology* (Nauka, Moscow, 2004), pp. 55−117 [in Russian].

2. V. Bondur, Complex Satellite Monitoring of Coastal Water Areas, 31.

3. V. G. Bondur and Yu. V. Grebenyuk, "Remote Indication of Anthropogenic Impacts on the Marine Environment Caused by Deep-Water Sewage Discharge: Modeling and Experiment," Issled. Zemli Kosmosa, No. 6, 1−19 (2001).

4. V. G. Bondur, Yu. V. Grebenyuk, E. V. Ezhova, et al., "Surface Manifestations of Internal Waves Investigated by a Subsurface Buoyant Jet. Part 1. The Mechanism of Internal-Wave Generation," Izv. Akad. Nauk, Fiz. Atmos. Okeana 45 (6), 833−845 (2009) [Izv., Atmos. Ocean. Phys. 45 (6) 779−790 (2009)].

5. V. G. Bondur, Yu. V. Grebenyuk, E. V. Ezhova, et al., "Surface Manifestations of Internal Waves Investigated by a Subsurface Buoyant Jet: Part 2. Internal Wave Field," Izv. Akad. Nauk, Fiz. Atmos. Okeana 46 (3) (2010) [Izv., Atmos. Ocean. Phys. 46 (3) (2010)] (in press).

6. R. J. Adrian, "Particle Imaging Techniques for Experimental Fluid Mechanics," Annu. Rev. Fluid Mech. 23, 261−304 (1991).

7. S. A. Ermakov, S. V. Kiyashko, and I. R. Konnov, "Determining the Elasticity Parameter of Surfactant Films from Damping Measurements of Standing Gravity−Capillary Waves," Izv. Akad. Nauk, Fiz. Atmos. Okeana 32 (4), 544−547 (1996) [Izv., Atmos. Ocean. Phys 32 (4), 503−505 (1996)].

8. S. A. Ermakov and S. V. Kijashko, "Laboratory Study of the Damping of Parametric Ripples due to Surfactant Films," Marine Surface Films, Gamburg: Springer, 113−128 (2006).

9. V. G. Levich, *Physicochemical Hydrodynamics* (FML, Moscow, 1959) [in Russian].

10. A. Kh. Naife, *Perturbation Methods* (Mir, Moscow, 1976) [in Russian].

11. E. Gossard and W. Hooke, *Waves in the Atmosphere* (Elsevier, Amsterdam, 1975; Mir, Moscow, 1978).

12. Yu.I. Troitskaya, D.A. Sergeev, E.V. Ezhova, I.A. Soustova, and V.I. Kazakov, Autogeneration of Internal Waves by Buoyant Surface Jets in a Stratified Basin, Dokl. Akad. Nauk 419 (5) 691−695 (2008).

13. K. Hasselmann, "On the Non-Linear Energy Transfer in a Gravity-Wave Spectrum. Part 1. General Theory," J. Fluid Mech. 12, 481−500 (1962).

14. T. Hara and W. J. Plant, "Hydrodynamic Modulation of Short Wind-Wave Spectra by Long Waves and Its Measurement Using Microwave Backscatter," J. Geophys. Res. 99 (C5), 9767−9784 (1994).

15. W. C. Keller and J. W. Wright, "Microwave Scattering and the Straining of Wind Generated Waves," Radio Sci. 10, 139−147 (1975).

16. W. J. Plant, "A Relationship between Wind Stress and Wave Slope," J. Geophys. Res. 87 (C3) 1961−1967 (1982).

17. O. M. Phillips, "The Equilibrium Range in the Spectrum of Wind Generated Water Waves," J. Fluid Mech. 4, 426−434 (1958).

18. S. A. Ermakov and S. G. Salashin, "Effect of Strong Modulation of Gravity−Capillary Waves by Internal Waves," Dokl. Akad. Nauk 337 (1), 108−111 (1994).

19. S. A. Ermakov, I. A. Sergievskaya, Yu. B. Shchegolkov, et al., "Wave Tank Study of "Cascade" Modulation of Bound Capillary−Gravity Waves due to Internal Waves," Proc. IGARSS. IEEE III, 1087−1089 (2000).

20. M. Gade, W. Alpers, S. A. Ermakov, et al., "Wind−Wave Tank Measurements of Bound and Freely Propagating Short Gravity-Capillary Waves," J. Geophys. Res. 103 (C9), 21697−21710 (1998).

21. W. J. Plant, W. C. Keller, V. Hesany, et al., "Bound Waves and Bragg Scattering in a Wind Wavetank," J. Geophys. Res. 104 (C2), 3243−3263 (1999).

22. W. J. Plant, "A New Interpretation of Sea-Surface Slope Probability Density Functions," J. Geophys. Res. 108 (C9), 3295, doi: 10.1029/2003JC001870 (2003).